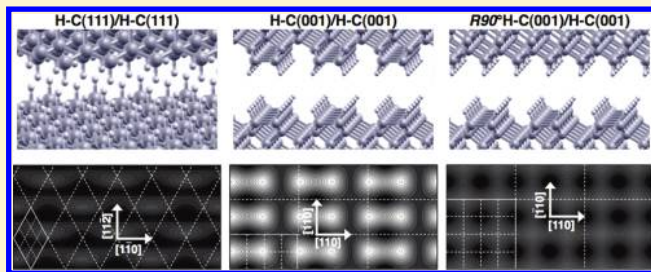


Ab Initio Calculation of the Adhesion and Ideal Shear Strength of Planar Diamond Interfaces with Different Atomic Structure and Hydrogen Coverage

G. Zilibotti and M. C. Righi*

Dipartimento di Fisica, Università di Modena e Reggio Emilia, Italy, and CNR-Istituto di Nanoscienze, Centro S3, Modena, Italy

ABSTRACT: We propose a method to calculate the ideal shear strength τ of two surfaces in contact by ab initio calculations. This quantity and the work of adhesion γ are the interfacial parameters usually derived from tip-based friction force measurements. We consider diamond interfaces and quantitatively evaluate the effects of surface orientation and passivation. We find that in the case of fully passivated interfaces, γ is not affected by the orientation and the alignment of the surfaces in contact. On the contrary, τ does show a dependence on the atomic-scale roughness of the interface. The surface termination has a major impact on the tribological properties of diamond. The presence of dangling bonds, even at concentrations low enough to prevent the formation of interfacial C–C bonds, causes an increase in the resistance to sliding by 2 orders of magnitude with respect to the fully hydrogenated case. We discuss our findings in relation to experimental observations.



INTRODUCTION

Understanding friction on the microscopic level is a fundamental problem with important practical applications. On the nanoscale, in particular, the dominance of the surface over the bulk renders the control of adhesion, friction, and wear essential to the development of devices with moving components such as micro- and nanoelectromechanical systems (MEMS/NEMS). Many experimental studies in nanotribology are carried out by means of the atomic force microscope (AFM), which provides a single-asperity contact with the substrate. The physical quantities usually derived are the interfacial work of adhesion γ (i.e., the work per unit area required to separate the surfaces from contact to infinity¹) and the interfacial shear strength τ , which has dimensions of frictional force per unit area and describes the intrinsic resistance to sliding of an interface.² These quantities are commonly determined by fitting the results of friction force measurements to contact mechanics models.³

In this article, we apply first principle density functional theory (DFT) calculations to obtain γ and τ for two planar diamond surfaces in contact with one another. The calculated values should be regarded as limiting values because the simulated surfaces are commensurate and infinitely flat. Nevertheless, they can provide useful information for understanding the effects of different surface properties on the tribological performance. In this work, we consider, in particular, the effects of surface atomic structure and passivation on diamond tribology.

Diamond is an excellent material for tribological applications, both on the macroscale and on the nanoscale, where it is considered to be a very promising substitute for silicon in MEMS/NEMS.^{4,5} Diamond tribology has been the subject of many experimental^{6–13} and theoretical^{6,14–23} studies. A comparison of

different sliding directions and surface orientations was performed by means of AFM and classical molecular dynamics (MD).⁶ The hydrogen-terminated H–C(111)-(1 × 1) and H–C(001)-(2 × 1) surfaces were considered. AFM measurements, carried out with hydrogenated amorphous tips, showed higher adhesion and friction forces for (001) versus (111) surfaces. The increased friction forces were attributed to a higher contact area due to the higher adhesion, thus no significant differences were reported for the shear strength, in agreement with the MD simulations. In another AFM-based study, the friction of a diamond tip on hydrogenated (111) and (001) surfaces presented similar intensities on both surfaces and turned out to be almost independent of the sliding direction and the load.⁷ Classical MD simulations of self-mated, planar (111) surfaces^{14,15} and (001) surfaces¹⁶ predicted a slight frictional anisotropy and a similar frictional dependence on load for both surfaces. These results deviate from macroscopic observations.^{8–10} Friction and wear measured for the (111) surface are usually lower than for the (001) surface, which also exhibits marked anisotropy. Concerning the effects of surface passivation, it is well established both experimentally^{11–13} and theoretically^{17–23} that surface termination by hydrogen or other adsorbates, such as dissociated water molecules, present in humid air reduces friction and diamond wear.

Here we evaluate the effects of the surface atomic structure by quantitatively comparing γ and τ calculated for three interfaces obtained by mating fully hydrogenated diamond surfaces with

Received: March 1, 2011

Revised: April 18, 2011

Published: May 05, 2011

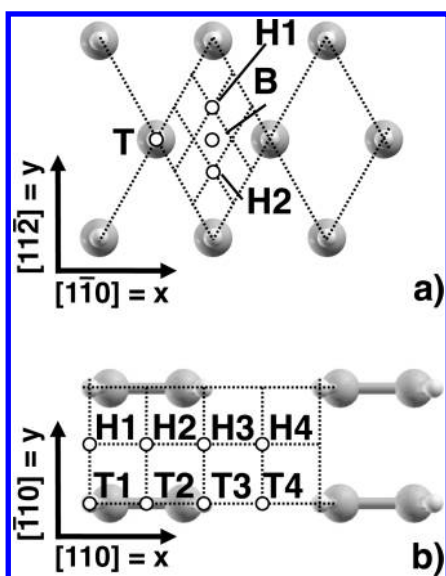


Figure 1. Bidimensional representations of the unit cells used to simulate the (a) H-C(111) and (b) H-C(001) surfaces. The grids employed to construct the PESs of the corresponding sliding interfaces are also represented. (See the text.)

different orientations/reconstructions and relative alignment: H-C(111)/H-C(111), H-C(001)/H-C(001) and $R90^\circ\text{H-C}(001)/\text{H-C}(001)$. The latter consists of two H-C(001) surfaces rotated by 90° , one with respect to the other. In investigating the effects of surface passivation, we focus on one interface structure, H-C(001)/H-C(001), and we vary the hydrogen coverage. We consider, in particular, $\theta_{\text{H}} = 75\%$, $\theta_{\text{H}} = 50\%$, and $\theta_{\text{H}} = 0$, which coincides with a bare C(001)/C(001) interface.

METHOD

We perform plane wave/pseudopotential calculations.²⁴ The approximation for the exchange-correlation functional is selected by performing test calculations on the structural and electronic properties of bulk diamond: we compared the local density approximation (LDA) to the generalized gradient approximation (GGA) in two different parametrizations, PW91²⁵ and PBE.²⁶ The results obtained with PBE turn out to be in closest agreement with experiments.²⁰ The ionic species are described by ultrasoft pseudopotentials, and the electronic wave functions are expanded in a plane-wave basis. On the basis of test calculations, we use a cutoff of 30 Ry to truncate the expansion.

We consider the (111) and (001) surfaces of diamond with hydrogen termination. The most stable phase for the H-C(111) surface is the dereconstructed (1×1) surface presenting a hydrogen atom on top of each surface carbon atom, whereas H-C(001) presents a (2×1) reconstruction consisting of monohydrogenated carbon dimers.^{27,28} A representation of the 2D cells used to simulate the surfaces is reported in Figure 1. The k points used in the calculations are generated through the Monkhorst Pack (MP) algorithm.²⁹ A $(10 \times 10 \times 1)$ MP grid is used to sample the Brillouin zone of the (111) surface, and a $(5 \times 10 \times 1)$ MP grid is used for the (001) surface.

The system consisting of two interacting surfaces, from now on referred to as the “interface”, is simulated by periodic supercells containing two slabs in contact and a vacuum region of 30 Å that separates the periodic replicas along the z direction. Test calculations revealed that slab thicknesses corresponding to 12 and 9 carbon layers are sufficient to

simulate the (111) and (001) surfaces, respectively. The external layers of the contacting slabs are hydrogen-terminated.

The interaction energy of the two mating surfaces is calculated to be $\nu = (E_{12}^{\text{tot}} - E_{1+2}^{\text{tot}})$, where E_{12}^{tot} is the energy of the supercell containing two interacting slabs at the equilibrium distance and E_{1+2}^{tot} is the energy of the supercell containing two noninteracting slabs (i.e., two slabs separated by a vacuum region that is 15 Å thick on both sides). We calculate ν for different relative lateral positions of the two surfaces, constructing in this way the potential energy surface (PES) experienced by a surface cell when translating along the substrate. Figure 1a shows the homogeneous grid adopted to construct the PES for the H-C(111)/H-C(111) interface. Each grid point indicates the position of the hydrogenated carbon atom of the upper surface (not shown) within the substrate unit cell. Four symmetry points of the hexagonal lattice are selected, namely, the top site T, the bridge site B, and the two hollow sites H1 and H2. The latter two sites differ in the position of the carbon atom immediately below the surface layer (the first layer): H1 is located above a C atom of the second layer and H2 is above a C atom of the third layer. In Figure 1b, the grid used to sample the (2×1) cell of the H-C(001)/H-C(001) interface is shown. Each point indicates the position of the center of a dimer of the sliding surface within the (2×1) cell of the substrate. The grid points are labeled by T to indicate that they belong to a top sliding channel where their superimposition between the dimers of the two surfaces is higher and by H to indicate that they belong to a hollow sliding channel where the superimposition between the dimers of the two surfaces is lower. The $R90^\circ\text{H-C}(001)/\text{H-C}(001)$ interface is simulated by using a (2×2) cell. In this case, the dimers of the sliding surface lie along the $[\bar{1}10]$ direction (i.e., perpendicularly to the dimers of the substrate surface).

A structural relaxation of the system is performed at each lateral position by keeping fixed the three bottom layers of the lower slab and optimizing all the degrees of freedom except for the (x, y) coordinates of the three topmost layers of the upper slab. In this way, during the relaxation the distance between the two surfaces (initially fixed to 1.5 Å between the atoms belonging to the interfacial layers) could reach its equilibrium value, z_{eq} , at each fixed lateral position. The PES, $\nu(x, y, z_{\text{eq}})$, is obtained through a bicubic interpolation of the calculated energies. The PES absolute minimum defines the work of adhesion: $\gamma = -\nu_{\text{min}}/A$, where A is the area of the surface unit cell ($A = 12.8 \text{ \AA}^2$ for the (001) surface and $A = 5.5 \text{ \AA}^2$ for the (111) surface). The PES absolute maximum defines the potential corrugation $\Delta\nu = \nu_{\text{max}} - \nu_{\text{min}}$. The lateral force f_α experienced by a surface unit cell during its displacement along the direction α is obtained as $f_\alpha = -\nabla_\alpha \nu$. We register the most negative value, f_α^s , of the periodic function f_α as the maximum resistance to sliding along the considered direction. The interfacial shear strength is then obtained as $\tau_\alpha^s = f_\alpha^s/A$. The superscript s , which will be abandoned from now on, indicates that the calculated shear strength is obtained from the static friction force and not from the kinetic one.

RESULTS

Effects of Interfacial Atomic-Scale Roughness. The effects of the interfacial atomic structure on the adhesion and shear strength are investigated by considering the fully hydrogen-terminated interfaces represented in Figure 2a. The interface obtained by self-mating H-C(111) surfaces (left panel) is smoother than the interface obtained by self-mating H-C(001) surfaces identically aligned (center panel). In this case, parallel dimer rows shape deep interfacial trenches. The latter ones disappear if one surface is rotated by 90° with respect to the other one (right panel). In spite of the different morphology, we find that the three different pairs of surfaces present the same equilibrium separation and similar adhesion energies. These

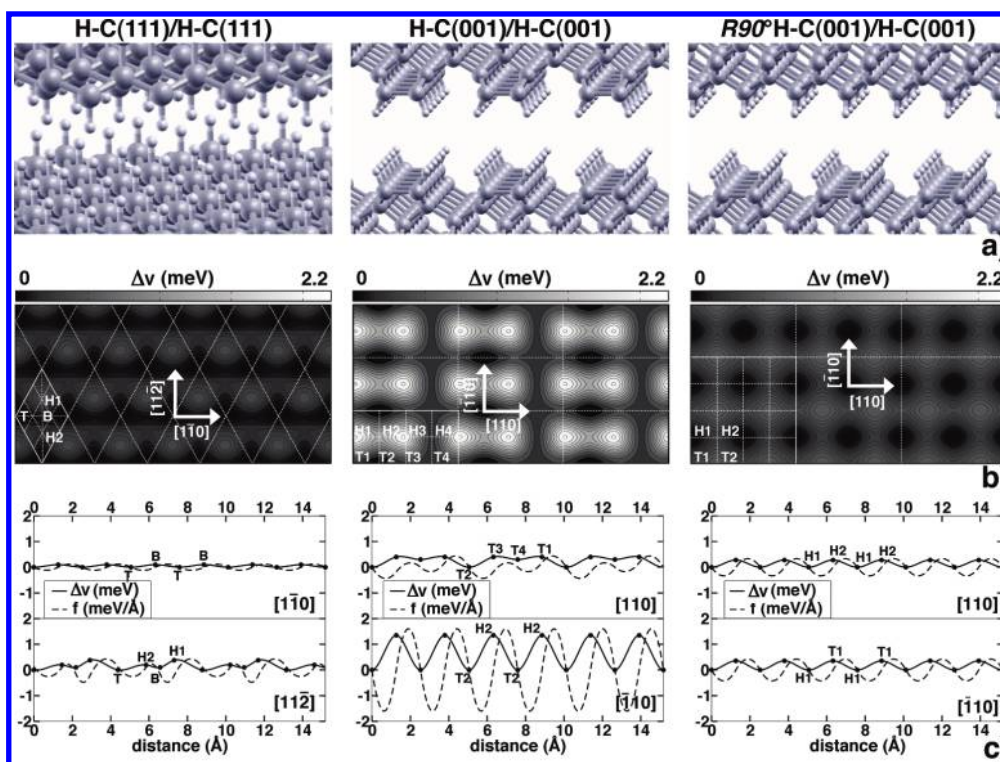


Figure 2. (a) Ball-and-stick representation of the three considered hydrogen-terminated diamond interfaces. (b) The corresponding PESs are reported below each structure. The grayscale indicates the variation of the surface interaction energy per (1×1) contact Δv with respect to its minimum value. A common energy scale is used for comparison. (c) The potential profile (—) and the lateral force (---) per (1×1) contact plotted as a function of the surface relative displacement along the symmetry directions indicated by the arrows on the PESs.

properties are clearly determined by the identical termination of the considered surfaces. The CH bonds of H-C(001) and H-C(111) surfaces present almost the same polarization: the calculated Löwdin charges³⁰ indicate that the hydrogen atoms on the H-C(001) (H-C(111)) surface present a charge depletion of $\delta_{\text{H}} = +0.16e$ ($+0.15e$) whereas the carbon atoms present an extra charge of $\delta_{\text{C}} = -0.14e$ ($-0.13e$) with respect to the valence charges. The polarization, the orientation, and the length ($d_{\text{CH}} = 1.05 \text{ \AA}$) of the CH bonds remain essentially unchanged when two surfaces are brought into contact. The presence of a layer of fully saturated polar bonds produces high repulsion between the surfaces at small separation. We observed, in fact, that during the process of structural relaxation, the two surfaces, initially positioned 1.5 \AA apart, increase their separation until the top surface, which is free to move along the z direction, reaches a distance of $z_{\text{eq}} = 3 \text{ \AA}$ between the terminating H atoms of the two surfaces in contact. Identical equilibrium separations are obtained for all three considered interfaces. The corresponding interaction energies, which are a few millielectronvolts per (1×1) cell, are reported in Table 1. The negative sign indicates adhesion between the surfaces. It is well known that DFT calculations based on LDA, or equally on GGA where the exchange-correlation energy is a functional of the local electronic density, are not able to describe the nonlocal part of van der Waals interactions accurately. The adhesion energies reported in Table 1 should then be considered to be affected by an error whose magnitude depends on the chosen approximation of the exchange correlation functional. However, the trends highlighted by the comparison of the results can be considered to be reliable. Furthermore, the description offered by the present calculations seems to be

not too far from reality: the work of adhesion measured for a diamond tip on a fully hydrogenated ultrananocrystalline diamond surface,¹³ $\gamma = 10 \text{ mJ/m}^2$, is in very good, maybe fortuitous, agreement with our results (Table 1). In the case of H-C(111)/H-C(111), we obtain the same value calculated by Qi et al. by means of DFT-GGA(PW91) calculations.¹⁹ The work of adhesion γ values obtained for the three considered interfaces are very similar. This finding differs from that reported by Gao et al.: by interpreting the results obtained by AFM measurements, they estimated work of adhesion values that were 45–60% lower for the H-C(111) surface than for the H-C(001) surface.⁶ Such a large difference cannot be accounted for by the difference in tip–surface interaction caused by the different arrangement of C–H bonds on the two surfaces. If the surfaces considered in the experiments are not substantially dissimilar from the crystalline surfaces considered here, then a possible reason for the different adhesion values measured on H-C(111) with respect to H-C(001) could be a different degree of passivation, even caused by H desorption during the tribological test. The energy required to create a dangling bond on the H-C(001) surface is, in fact, lower than that on the H-C(111) surface.³¹

We consider now the influence of the interfacial atomic-scale roughness on the PES shape. A bidimensional representation of the PESs obtained for the three considered interfaces is shown in Figure 2b. The grayscale indicates the variation of the surface interaction energy as a function of the relative lateral position. The absolute minimum (in black) is taken as a reference, and a common energy scale is used. The corrugation Δv of each PES is reported in Table 1. By comparing Figure 2a,b, one can readily see that the PES shape exactly resembles the interface shape. This

Table 1. Interaction Energy Calculated for the Surface Relative Position Corresponding to the PES Absolute Minimum, $v_{\min} = v([x, y]_{\min}, z_{\text{eq}})$ ^a

interface	(1 × 1) contact			interfacial	
	v_{\min} (me V)	Δv (me V)	f_x^s, f_y^s (pN)	γ (mJ/m ²)	τ_x, τ_y (MPa)
H–C(111)/H–C(111)	–2.8	0.4	0.2, 0.7	7.9	3.6, 12.6
H–C(001)/H–C(001)	–3.8	2.2	0.7, 2.6	9.4	10.9, 40.6
R90°H–C(001)/H–C(001)	–4.7	0.5	0.5, 0.7	11.8	7.8, 10.9

^a The PES corrugation Δv and the maximum restoring forces along symmetry directions (Figure 1) are reported per (1 × 1) cell. The corresponding interfacial quantities (i.e., the work of adhesion γ and shear strength τ) are also reported. Fully hydrogenated interfaces having different atomic structures are compared.

result suggests that the atomic-scale roughness may play a role on the nanoscale similar to that played by the macroscopic roughness in influencing the frictional properties of systems. The PES obtained for the H–C(001)/H–C(001) interface presents a corrugation that is about 6 times higher than the PES corrugation obtained for the smoother H–C(111)/H–C(111) interface (Table 1). The PES presents features of the substrate structure convoluted by the slider structure. Thus, by rotating the slider with respect to the substrate, as in the case of the R90°H–C(001)/H–C(001) interface, the PES is smoothed and becomes as flat as the H–C(111)/H–C(111) PES.

The differences observed in the PES corrugation and anisotropy appear in the frictional forces. In Figure 2c, we report the potential profiles experienced by the slider when it is displaced from the PES absolute minimum and moved along the two symmetry directions indicated by arrows. In the case of the (001) surface, we consider the [110] and $[\bar{1}10]$ directions, which are minimum-energy paths (MEPs) because they connect PES minima passing through saddle points. In the case of the hexagonal lattice, we consider the [110] and $[11\bar{2}]$ directions. The latter path is considered for comparison even if it is not an MEP because it passes thorough the PES maxima. The lateral forces acting on the slider unit cell when displaced from the PES absolute minimum and dragged along the considered directions are represented in Figure 2c with dashed lines. The maximum values recorded for the restoring forces, f_{ω}^s , are reported in Table 1. We can observe that static friction does not exhibit any significant dependence on the sliding orientation in the case of H–C(111)/H–C(111) and the R90°H–C(001)/H–C(001) interfaces. On the contrary, for the anisotropic H–C(001)/H–C(001) interface f_x^s is about four times lower than f_y^s : when sliding along the [110] direction, the dimers of the upper surface remain within a top sliding channel, whereas when sliding along the $[\bar{1}10]$ direction they alternately cross top and hollow sliding channels, which produces rapid variations of the surface interaction energy and thus higher frictional forces.

The calculated shear strengths are on the order of megapascals (Table 1), in particular, a few megapascals on average for H–C(111)/H–C(111) and R90°H–C(001)/H–C(001) and a few tens of megapascals for H–C(001)/H–C(001). Thus, our calculations predict better tribological performances for atomically smoother diamond interfaces: a slider, like an AFM tip, should slide more easily on the H–C(111) surface than on the H–C(001) surface if the two surfaces present the same hydrogen termination. This result is in agreement with macroscopic observations⁸ but deviates from that reported by Gao et al., who attributed the higher frictional forces measured by AFM on the (001) surface with respect to those on the (111) surface to a

higher contact area due to higher adhesion, obtaining in this way similar shear strengths for the two surfaces of about 100 MPa.

Effects of Dangling Bonds. Abundant hydrogen is present in CVD processes, thus diamond surfaces obtained by this growth technique are mostly hydrogen-terminated.³² First principles calculations of surface energy showed, in fact, that the hydrogen-terminated phase of both the (001) and the (111) surfaces of diamond is more stable than the bare phase.³³ During surface sliding, carbon dangling bonds (DBs) can be produced on hydrogenated surfaces by mechanical rubbing, and their presence can cause a significant frictional increase as observed in tribological tests carried out in vacuum or under dry conditions.^{34,35} Here we quantitatively analyze the effects of DBs on the adhesion and shear strength. Toward this aim, we consider the H–C(001)/H–C(001) interface and realize different interfacial densities of DBs. In particular, we simulate three different hydrogen coverages: $\theta_{\text{H}} = 75\%$, obtained by including one DB per interface cell; $\theta_{\text{H}} = 50\%$, with two DBs per cell; and $\theta_{\text{H}} = 0$, obtained by self-mating two clean C(001) surfaces. The latter system may be representative of a situation where a high density of DBs is present. The optimized configuration of the partially hydrogenated interfaces is shown in Figure 3a. Under conditions of low DB concentration, where carbon bonds are not established at the interface as in the case of $\theta_{\text{H}} = 75\%$, the surface equilibrium distance is reduced with respect to the fully hydrogenated conditions (Figure 3a, left panel) and the attractive interaction between the surfaces is slightly increased (Table 2). The curve representing the interaction energy as a function of the surface separation $v([x, y]_{\min}, z)$ presents, in fact, a deeper minimum that is shifted toward shorter distances with respect to the fully hydrogenated interfaces.³⁶ The nature of the surface interaction is completely altered when the DB density becomes high enough to allow the formation of covalent bonds at the interface, as happens for $\theta_{\text{H}} = 50\%$ (Figure 3a, central panel). In this case, the work of adhesion increases by 3 orders of magnitude with respect to the fully passivated interfaces (Table 2). The formation of a C–C bond at the interface was possible in our quasi-static calculations thanks to the short distance between the slabs selected for the starting configuration of the relaxation process. The interaction between two bare diamond surfaces, $\theta_{\text{H}} = 0$, results in a cold welding of the surfaces, even if a stable surface reconstruction is present on the surfaces in contact (Figure 3a, right panel).

The increase in the adhesion energy caused by the presence of carbon DBs at the interface is accompanied by a corresponding increase in the PES corrugation. By comparing Tables 1 and 2, we can observe that Δv increases by about 1 order of magnitude in the presence of a 25% density of DBs with respect to full

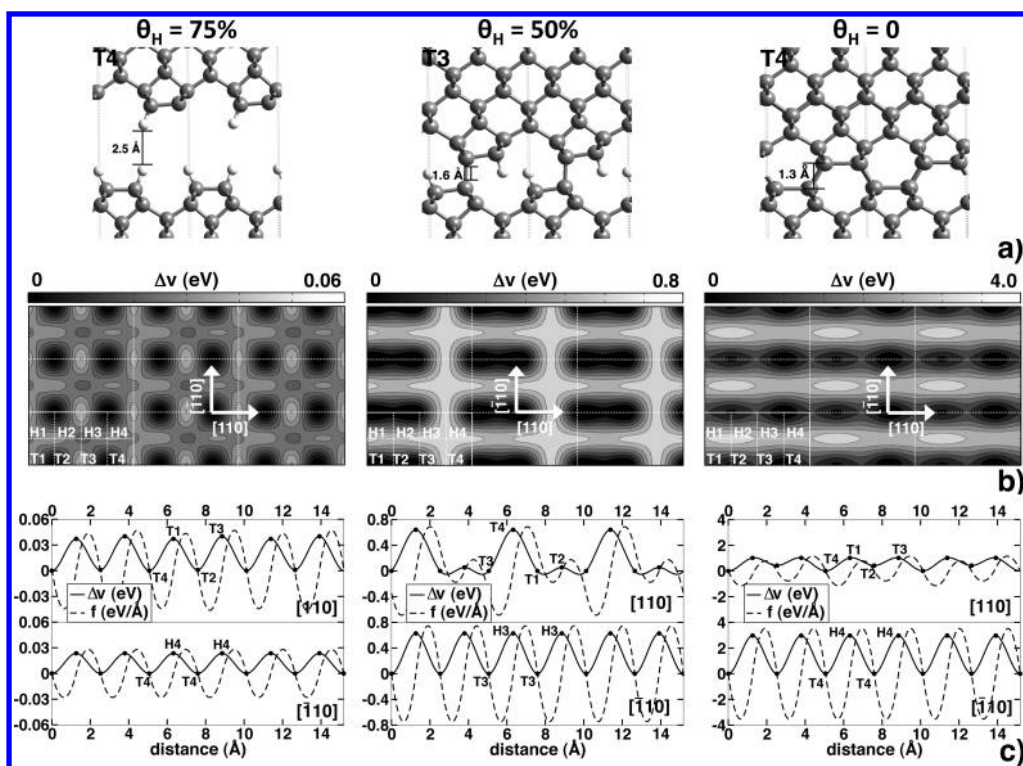


Figure 3. (a) Lateral view of the interfacial configurations corresponding to the minimum interaction energy between partially passivated diamond (001) surfaces. θ_H indicates the interfacial hydrogen coverage. (b) Calculated PESs. Different energy scales are used. (c) Potential profiles and lateral forces per (1×1) contact along the $[110]$ and $[\bar{1}10]$ directions.

Table 2. Interaction Energy Calculated for the Surface Relative Position Corresponding to the PES Absolute Minimum, $\nu_{\min} = \nu([x, y]_{\min}, z_{\text{eq}})^a$

interface	(1×1) contact			interfacial	
	ν_{\min} (eV)	$\Delta\nu$ (eV)	f_x^s, f_y^s (nN)	γ (J/m ²)	τ_x, τ_y (GPa)
$\theta_H = 0.75$	-0.005	0.04	0.08, 0.05	0.01	1.3, 0.8
$\theta_H = 0.50$	-0.6	0.6	1.1, 1.2	1.6	17.2, 18.8
$\theta_H = 0$	-3.0	3.3	1.8, 5.6	7.5	28.1, 87.5

^aThe PES corrugation $\Delta\nu$ and the maximum restoring forces along symmetry directions (Figure 3) are reported per (1×1) cell. The corresponding interfacial quantities (i.e., the work of adhesion γ and the shear strength τ) are also reported. Interfaces obtained by self mating two (001) diamond surfaces presenting different interfacial H coverages, θ_H , are compared.

hydrogenation. And the presence of a 50% density of DBs produces a PES corrugation that is 3 orders of magnitude higher. The modifications in the PESs caused by the presence of carbon DBs are clearly visible in Figure 3b (Note that different energy scales are used for the three different interfaces.) The presence of carbon DBs on both mating surfaces shapes deep minima in the PES located at the grid points corresponding to the surface relative positions where covalent carbon bonds are established, namely, T3 for the $\theta = 50\%$ interface and T4 for the $\theta = 0$ interface. This is clearly visible in the potential profiles reported in Figure 3c: to displace the top surface from position T3 (T4), a lateral force of $f_x = 1.1$ nN ($f_x = 1.8$ nN) per (1×1) surface cell is necessary. The situation is even worse if the displacement occurs along the direction perpendicular to the dimers, the y direction,

causing a higher detachment of the surfaces in correspondence with the hollow channels. This situation gives rise to a high friction anisotropy, which is particularly evident in PES obtained for the bare diamond interface that presents high- and low-energy channels in correspondence with the hollow and top sliding channels, respectively. The calculated shear strengths for H-depleted surfaces presenting interfacial C–C bonds are on the order of gigapascals (Table 2) (i.e., three orders of magnitude higher than the shear strengths obtained for fully passivated interfaces). In the case of the bare interface, τ approaches the ideal shear strength calculated for bulk diamond, which is 93 GPa.³⁷ It has recently been shown by molecular dynamics that the sliding of two unsaturated diamond surfaces leads to the gradual destruction of the surfaces.³⁸ The resulting amorphous interface layer grows with a rate that strongly depends on the surface orientation and sliding direction, in agreement with the experiments.^{8,39}

CONCLUSIONS

We present a method to calculate the ideal interfacial shear strength τ by ab initio calculations. In particular, we construct the potential energy surface (PES) that describes the variation of the adhesion energy γ between two surfaces in contact as a function of their relative lateral position. We then select relevant minimum energy paths and calculate the $T = 0$ static friction force as the maximum resistance to climbing the PES along the selected directions. These forces, normalized to the area of the contact, gives the shear strength, which we define as ideal because the considered interfaces are commensurate and infinitely flat. We apply this method to diamond, and we quantitatively evaluate the

effects of the interfacial atomic structure and the degree of passivation on γ and τ .

We find that the adhesion of fully passivated surfaces is not affected by their orientation and relative alignment. On the contrary, the shear strength is found to be more sensitive to the interfacial morphology. In particular, we find that the PES corrugation directly reflects the interface atomic roughness. The shear strengths obtained for the smooth H–C(111)/H–C(111) and R90°H–C(001)/H–C(001) interfaces are less than 10 MPa whereas in the case of the atomically rougher H–C(001)/H–C(001) interface the calculated τ is more than double on average. The structural anisotropy characterizing this latter interface gives rise to a frictional anisotropy that is almost absent in the other two interfaces.

A major impact on the intrinsic resistance to sliding of diamond interfaces is caused by the presence of dangling bonds. When decreasing the interfacial hydrogen coverage of H–C(001)/H–C(001) to $\theta_{\text{H}} = 75\%$, the average shear strength increases by 2 orders of magnitude. This fact deserves attention because C–C bonds are not formed in our model interface at $\theta_{\text{H}} = 75\%$ coverage. For the lower hydrogen coverages considered, $\theta_{\text{H}} = 50$ and 0%, covalent bonds are formed between the surfaces and the increased adhesion (γ is on the order of J/m²) is accompanied by a corresponding increase in the interfacial shear strength that approaches the ideal shear strength of bulk diamond in the case of bare surfaces in contact.

ACKNOWLEDGMENT

This work is supported by MIUR through PRIN 2007 BL78N3. We thank the DEISA Consortium (www.deisa.eu), funded through EU FP7 project RI-222919, for support within the DEISA Extreme Computing Initiative.

REFERENCES

- (1) Israelachvili, J. N. *Intermolecular Surface Forces*; Academic Press: London, 1992.
- (2) Szlufarska, I.; Chandross, M.; Carpick, R. W. *J. Phys. D: Appl. Phys.* **2008**, *41*, 123001.
- (3) Enachescu, M.; van den Oetelaar, R.; Carpick, R.; Ogletree, D.; Flipse, C.; Salmeron, M. *Tribol. Lett.* **1999**, *7*, 73–78.
- (4) Auciello, O.; Pacheco, S.; Sumant, A.; Gudeman, C.; Sampath, S.; Datta, A.; Carpick, R.; Adiga, V.; Zurcher, P.; Ma, Z.; Yuan, H.-C.; Carlisle, J.; Kabius, B.; Hiller, J.; Srinivasan, S. *Microwave Mag., IEEE* **2007**, *8*, 61–75.
- (5) Grierson, D. S.; Carpick, R. W. *Nano Today* **2007**, *2*, 12–21.
- (6) Gao, G.; Cannara, R. J.; Carpick, R. W.; Harrison, J. A. *Langmuir* **2007**, *23*, 5394–5405.
- (7) Germann, G. J.; Cohen, S. R.; Neubauer, G.; McClelland, G. M.; Seki, H.; Coulman, D. *J. Appl. Phys.* **1993**, *73*, 163–167.
- (8) Hird, J. R.; Field, J. E. *Proc. R. Soc. London, Ser. A* **2004**, *460*, 3547–3568.
- (9) Schmitt, M.; Paulmier, D.; Huu, T. L. *Thin Solid Films* **1999**, *343–344*, 226–229.
- (10) Grillo, S. E.; Field, J. E. *J. Phys. D: Appl. Phys.* **2000**, *33*, 595.
- (11) Erdemir, A. *Surf. Coat. Technol.* **2001**, *146–147*, 292–297.
- (12) Konicek, A. R.; Grierson, D. S.; Gilbert, P. U. P. A.; Sawyer, W. G.; Sumant, A. V.; Carpick, R. W. *Phys. Rev. Lett.* **2008**, *100*, 235502.
- (13) Sumant, A. V.; Grierson, D. S.; Gerbi, J. E.; Carlisle, J. A.; Auciello, O.; Carpick, R. W. *Phys. Rev. B* **2007**, *76*, 235429.
- (14) Harrison, J. A.; White, C. T.; Colton, R. J.; Brenner, D. W. *Phys. Rev. B* **1992**, *46*, 9700–9708.
- (15) Harrison, J. A.; Colton, R. J.; White, C. T.; Brenner, D. W. *Wear* **1993**, *168*, 127–133.
- (16) Perry, M. D.; Harrison, J. A. *J. Phys. Chem.* **1995**, *99*, 9960–9965.
- (17) Dag, S.; Ciraci, S. *Phys. Rev. B* **2004**, *70*, 241401.
- (18) Gao, G. T.; Mikulski, P. T.; Chateaneuf, G. M.; Harrison, J. A. *J. Phys. Chem. B* **2003**, *107*, 11082–11090.
- (19) Qi, Y.; Konca, E.; Alpas, A. T. *Surf. Sci.* **2006**, *600*, 2955–2965.
- (20) Zilibotti, G.; Righi, M. C.; Ferrario, M. *Phys. Rev. B* **2009**, *79*, 075420.
- (21) Manelli, O.; Corni, S.; Righi, M. C. *J. Phys. Chem. C* **2010**, *114*, 7045–7053.
- (22) Guo, H.; Qi, Y.; Li, X. *Appl. Phys. Lett.* **2008**, *92*, 241921.
- (23) Guo, H.; Qi, Y. *Model. Simul. Mater. Sci. Eng.* **2010**, *18*, 034008.
- (24) Baroni, S.; Corso, A. D.; de Gironcoli, S.; Giannozzi, P. 2001, <http://www.pwscf.org>.
- (25) Perdew, J. P.; Chevary, J. A.; Vosko, S. H.; Jackson, K. A.; Pederson, M. R.; Singh, D. J.; Fiolhais, C. *Phys. Rev. B* **1992**, *46*, 6671–6687.
- (26) Perdew, J. P.; Burke, K.; Ernzerhof, M. *Phys. Rev. Lett.* **1996**, *77*, 3865–3868.
- (27) Kress, C.; Fiedler, M.; Schmidt, W. G.; Bechstedt, F. *Phys. Rev. B* **1994**, *50*, 17697–17700.
- (28) Kawarada, H.; Sasaki, H.; Sato, A. *Phys. Rev. B* **1995**, *52*, 11351–11358.
- (29) Monkhorst, H. J.; Pack, J. D. *Phys. Rev. B* **1976**, *13*, 5188–5192.
- (30) Szabo, A.; Ostlund, N. S. *Modern Quantum Chemistry: Introduction to Advanced Electronic Structure Theory*; Dover Publications: New York, 1996.
- (31) Zilibotti, G.; Corni, S.; Righi, M. C. *Tribol. Lett.* **2011** Submitted.
- (32) Ristein, J. *Surf. Sci.* **2006**, *600*, 3677–3689.
- (33) Stekolnikov, A. A.; Furthmüller, J.; Bechstedt, F. *Phys. Rev. B* **2002**, *65*, 115318.
- (34) Gao, G. T.; Mikulski, P. T.; Harrison, J. A. *J. Am. Chem. Soc.* **2002**, *124*, 7202–7209.
- (35) van den Oetelaar, R. J. A.; Flipse, C. F. J. *Surf. Sci.* **1997**, *384*, L828–L835.
- (36) Zilibotti, G.; Ferrario, M.; Bertoni, C. M.; Righi, M. C. *Comput. Phys. Commun.* **2010**, in press, doi:10.1016/j.cpc.2010.12.023.
- (37) Roundy, D.; Cohen, M. L. *Phys. Rev. B* **2001**, *64*, 212103.
- (38) Pastewka, L.; Moser, S.; Gumbsch, P.; Moseler, M. *Nat. Mater.* **2011**, *10*, 34.
- (39) Wilks, E. M.; Wilks, J. *J. Phys. D: Appl. Phys.* **1972**, *5*, 1902.